magnetochemistry

MDPI

Article

A High Pressure Investigation of the Order-Disorder Phase Transition and Accompanying Spin Crossover in $[FeL1_2](ClO_4)_2$ (L1 = 2,6-bis{3-methylpyrazol-1-yl}-pyrazine)

Helena J. Shepherd [1,*], George Tonge [1], Lauren E. Hatcher [2], Mathew J. Bryant [2], Jane V. Knichal [2], Paul R. Raithby [2], Malcolm A. Halcrow [3], Rafal Kulmaczewski [3], Kevin J. Gagnon [4] and Simon J. Teat [4]

1 School of Physical Sciences, University of Kent, Canterbury, Kent CT2 7NH, UK; gt88@kent.ac.uk
2 Department of Chemistry, University of Bath, Claverton Down, Bath BA2 7AY, UK; l.e.hatcher@bath.ac.uk (L.E.H.); m.bryant@bath.ac.uk (M.J.B.); j.v.knichal@bath.ac.uk (J.V.K.); p.r.raithby@bath.ac.uk (P.R.R.)
3 School of Chemistry, University of Leeds, Woodhouse Lane, Leeds LS2 9JT, UK; m.a.halcrow@leeds.ac.uk (M.A.H.); r.kulmaczewski@leeds.ac.uk (R.K.)
4 Advanced Light Source, Lawrence Berkeley National Laboratory, Berkeley, CA 94720, USA; kjgagnon@lbl.gov (K.J.G.); sjteat@lbl.gov (S.J.T.)
* Correspondence: h.j.shepherd@kent.ac.uk; Tel.: +44-122-7827-887; Fax: +44-122-7827-558

Academic Editor: Guillem Aromí
Received: 11 January 2016; Accepted: 2 February 2016; Published: 17 February 2016

Abstract: A high pressure single crystal X-ray diffraction and Raman spectroscopy study has revealed a similar mechanism for both thermal and pressure-induced spin crossover in $[FeL1_2](ClO_4)_2$ (L1 = 2,6-bis{3-methylpyrazol-1-yl}-pyrazine) and the concomitant anion order-disorder transition.

Keywords: spin-crossover; molecular materials; high pressure; order-disorder phenomena

1. Introduction

Structure-property correlations in spin crossover (SCO) materials have the power to reveal the origins of cooperative behavior during spin state switching. The high spin (HS) state has a significantly larger volume than the low spin (LS) state, caused by differences in occupation of anti-bonding molecular orbitals altering the metal-ligand bond distances in the complex [1]. The difference in molecular shape between HS and LS states and the long-range elastic interactions in the solid state that determine the ability of the lattice to accommodate that strain determine the degree of cooperativity in these materials, and may also influence whether or not SCO can occur at all [1,2]. Strongly cooperative systems favor abrupt, first-order thermal spin transitions, while weakly cooperative systems present more gradual SCO behavior [3,4].

In the case of Fe^{2+} SCO complexes, the Fe-L bond lengths decrease by *ca.* 0.2 Å on going from the HS to LS state. This typically manifests itself at the macroscopic scale as a change in volume of the material of between 2% and 10%. A deep understanding of what drives cooperativity, particularly in systems showing unusual SCO characteristics, provides an opportunity to exploit these features for the design of novel switchable materials with cooperativity tuned to specific requirements.

Order-disorder transitions, in which SCO is accompanied by a significant change in the long-range ordering of counter ions, solvent molecules and/or ligand conformation [5–8] are a particularly interesting class of systems from the point of view of understanding cooperativity and models have

been developed to explore them further [9]. In this latter study [9], the importance of detailed structural studies across a range of temperature (*i.e.*, not simply structures in HS and LS states alone) was specifically highlighted.

The molecular complex $[Fe(L1)_2]\cdot 2ClO_4$, **1**, (L1 = 2,6-bis{3-methylpyrazol-1-yl}pyrazine) is closely related to the family of spin crossover (SCO) active $[Fe(bpp)_2]^{2+}$ (bpp = 2,6-di{pyrazol-1-yl}pyridine) systems [10]. A previous SQUID magnetometry study of **1** revealed an unusual transition curve, consisting of two steps, separated not by a plateau as is often the case in stepped SCO materials [11], but rather by a change in gradient from an abrupt initial step (on cooling) followed by a much more gradual second step [12], as shown in Figure 1. The change in gradient occurs when *ca.* 50% of the iron centers have undergone SCO. A subsequent structural study [13] aimed to rationalize the relationship between an observed order/disorder transition in this material and the unusual two-step transition in this complex, and led to the development of an Ising-like Hamiltonian for coupled SCO and order-disorder processes [9]. At no temperature did the structural study identify any indication of symmetry breaking to an intermediate phase with long range order of HS and LS states. In the HS state at 210 K one of the two perchlorate anions was found to be highly disordered, while the other was fully ordered. At 180 K (after the initial abrupt step) both ions are fully ordered. It was suggested that the ordering of the second cation may reduce the cooperativity in the material, resulting in the gradual second step.

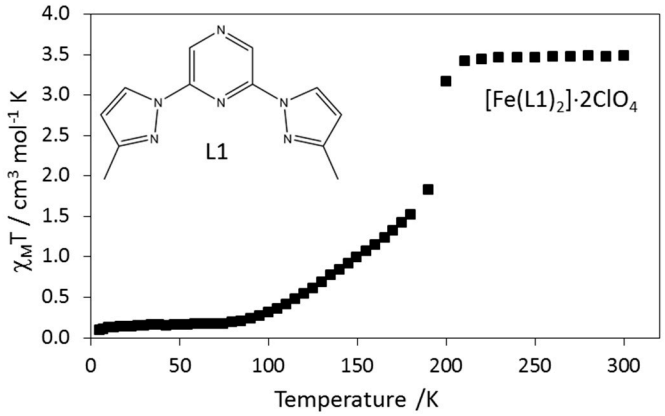

Figure 1. Variable temperature SQUID magnetometry data for **1** derived from those presented in ref. [12]. The inset shows the chemical structure of 2,6-bis{3-methylpyrazol-1-yl}pyrazine (L1).

The large difference in the metal-ligand bond lengths between HS and LS states imparts high sensitivity of SCO materials to pressure. Increasing pressure destabilizes the larger HS state, decreasing the energy barrier between the two states and thus shifts the transition to higher temperatures [14]. More generally, hydrostatic pressure can be used as a tool to probe structure-property correlations, often modifying crystallographic phase transitions and tuning intermolecular interactions without changing the chemical connectivity of the material. The latter point is particularly pertinent in the case of molecular SCO materials where both the chemical connectivity and the intermolecular interactions have strong influence on properties: small changes in chemistry of ligands can significantly alter switching properties, while different polymorphs of the same molecule can show vastly different SCO properties [15]. Pressure has also been used to decouple crystallographic phase transitions from SCO properties in order to probe their interrelationship [16].

With the aim of shedding further light on this material and indeed the coupling between order-disorder phenomena and SCO in general we performed a detailed series of variable temperature and pressure X-ray diffraction and Raman spectroscopic experiments on single crystal samples of **1**.

2. Results and Discussion

2.1. Variable Temperature and Pressure Raman Spectroscopy

Raman spectroscopy can be used to monitor the spin state of the material as a function of both temperature and pressure [17], with the intensities of selected "marker" peaks used to follow the SCO. The spectra of **1** at 273, 178 and 103 K (Figure 2a) clearly reflect the significant structural changes that occur during SCO. The spectra of **1** at ambient pressure inside the diamond anvil cell (DAC), at 10.0 and 28.8 kbar are also shown in Figure 2b.

The peaks at 653 cm^{-1} (marker for HS state) and 663 cm^{-1} (marker for LS state) were chosen to follow the spin state as a function of both temperature and pressure. A plot of the relative intensities of the two peaks as a function of temperature is shown in Figure 3; comparison with the magnetometry curve reveals the same abrupt/gradual profile of the SCO properties as expected if appropriate marker peaks are chosen. It should be noted that the intensity ratio is not necessarily directly proportional to the HS fraction, and thus quantification of the proportion of molecules in either spin state at a given temperature (or pressure) must be obtained from another method. This technique does however provide qualitative information regarding the overall shape of the SCO curve, and the relative simplicity of the experiment means much finer sampling over both temperature and pressure is viable.

Using the same spin state indicator peaks, a qualitative pressure-induced SCO curve can be determined as shown in Figure 3b. A similar overall shape is observed for both the thermal and pressure-induced processes; an abrupt initial step (intensity ratio decreases by *ca.* 60% within 2.5 kbar) centered at 10 kbar followed by a much more gradual second step indicating the remaining molecules undergo SCO over *ca.* 15 kbar. By 25 kbar the spin crossover process appears to be complete. The similarity of the full Raman spectra across the thermal and pressure-induced transitions (shown in Figure 2) also suggest that the mechanism of SCO is the same in both cases.

On warming back to room temperature or depressurization from 32 kbar the Raman spectra are indistinguishable from those before changing conditions, *i.e.* both the thermal and pressure-induced transitions are fully reversible.

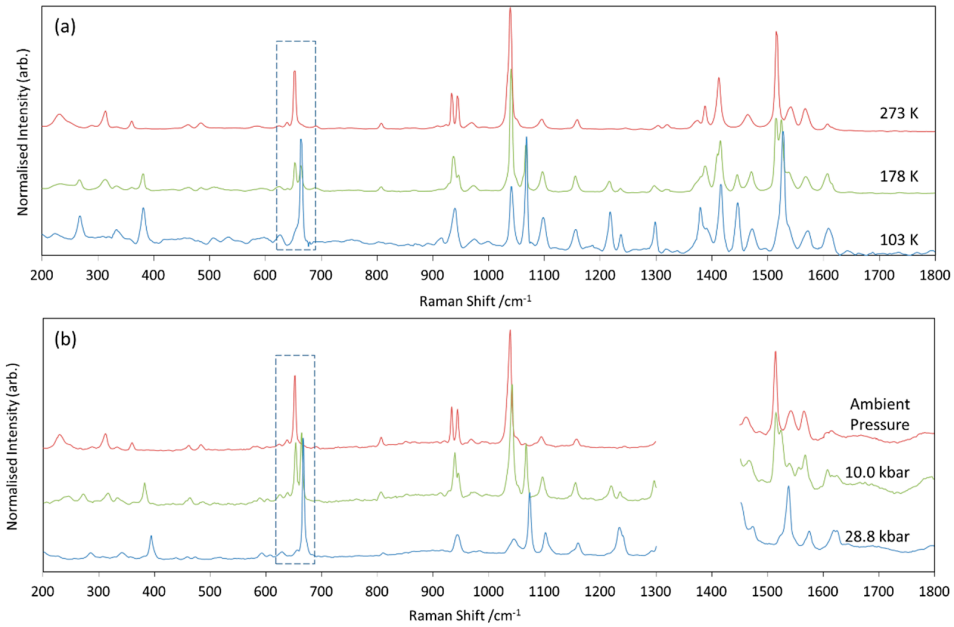

Figure 2. (**a**) Raman spectra of **1** at 273 178 and 103 K; (**b**) Raman spectra of **1** at ambient pressure inside the diamond anvil cell (DAC), at 10.0 and 28.8 kbar. The dashed box highlights the region of the HS and LS marker peaks (*ca.* 653 and 663 cm^{-1} respectively). The region between 1300 and 1450 cm^{-1} is obscured by intense diamond and ruby signals from the DAC during the high pressure study.

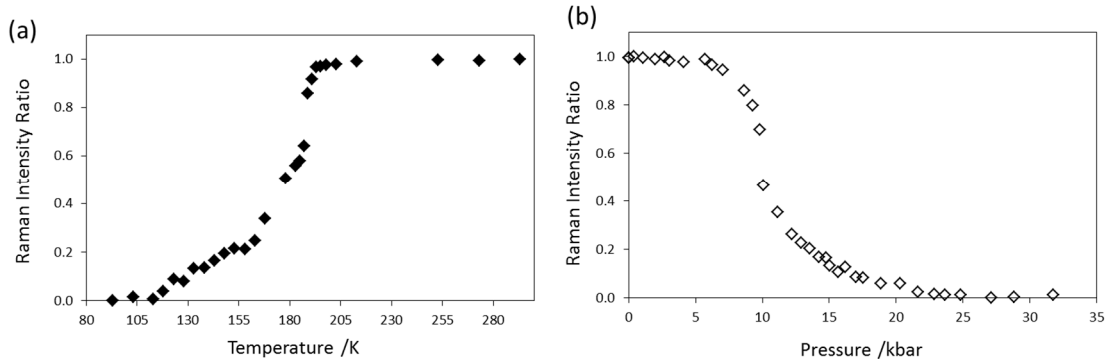

Figure 3. Relative intensities of peaks at 653 and 663 cm^{-1} (**a**) as a function of temperature; (**b**) as a function of pressure at ambient temperature.

2.2. *Variable Temperature X-ray Diffraction*

The crystal structure was determined every 10 K on cooling from 270 to 100 K, allowing both steps of the transition to be investigated thoroughly. The structure at 270 K is shown in Figure 4a, where the disorder of one of the two perchlorate anions is clearly visible. As O2 displays dynamic thermal disorder no attempt was made to model this motion over multiple discrete positions; it is evident that this perchlorate ion is tumbling. The Fe-N_6 coordination volume as a function of temperature is shown in Figure 4b, and again closely matches the curve from the magnetic data, with an abrupt decrease in the volume (equal to *ca.* 58% of the total volume change) occurring within 10 K, with a second gradual decrease in volume taking place over more than 80 K. The abrupt/gradual transition is also observed in the unit cell parameters (Figure 4c).

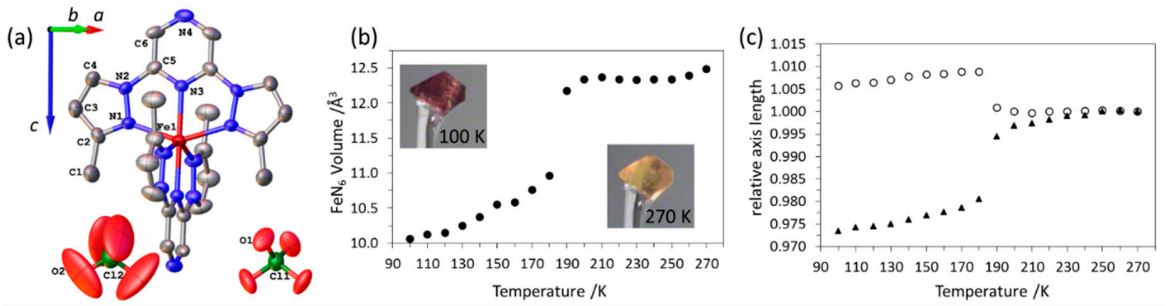

Figure 4. (**a**) Crystal structure of **1** at 270 K showing the numbering scheme used throughout for the crystallographically unique atoms. Atomic displacement parameters are shown at 50% probability and hydrogen atoms have been omitted for clarity; (**b**) Volume of the FeN_6 coordination polyhedron as a function of temperature. The insets show pictures of the crystal in the yellow HS state (at 270 K) and the brown LS state (at 100 K); (**c**) Evolution of the *a*- (▲) and *c*- (○) axes as a function of temperature, normalized to the 270 K value.

As in the previous study, no indication of symmetry breaking to an intermediate phase with long range order of HS and LS sites was observed. Nor were any supercell reflections observed at any temperature, precluding the possibility of cell doubling to an intermediate phase with long range order of spin states. Zone images of the (hk0) and (0kl) zones of reciprocal space recorded at 190 and 180 K are shown in Figure 5, demonstrating the lack of commensurate modulation accompanying the spin transition.

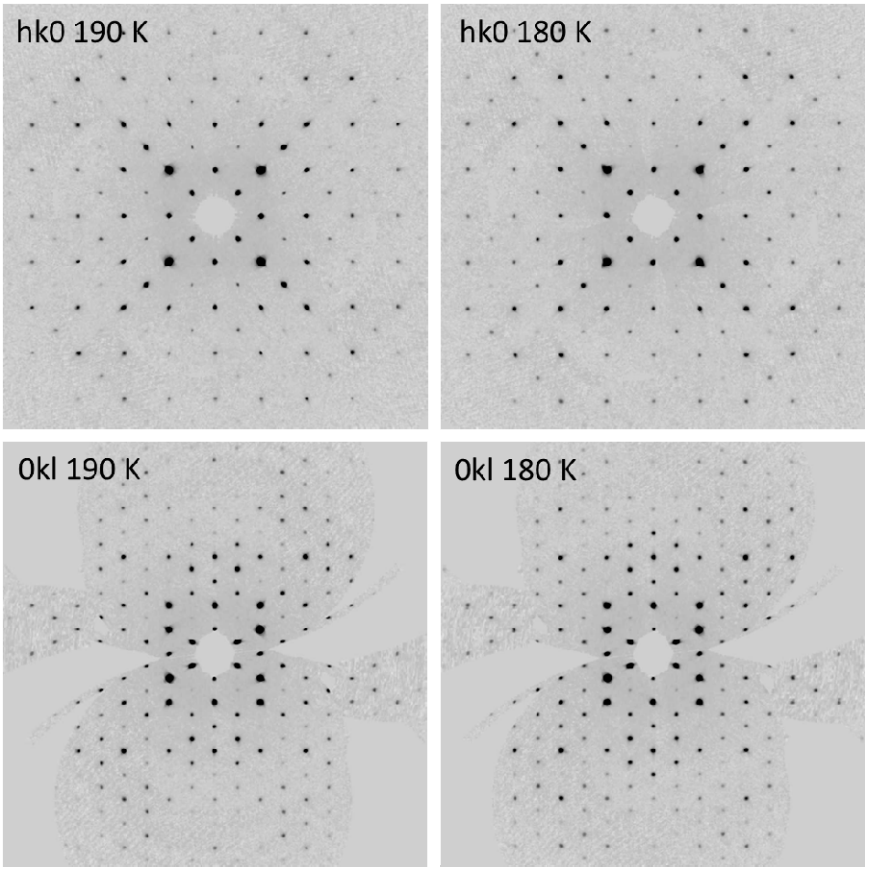

Figure 5. Images of the (hk0) zone at 190 K (top left) and 180 K (top right) and (0kl) zone at 190 K (bottom left) and 180 K (bottom right), demonstrating the lack of commensurate modulation after the initial abrupt step in the transition.

Conformational changes have previously been suggested as the origin of cooperative properties in some related SCO complexes with bpp ligands [1,2,18]. In the case of **1**, the angle between the mean-planes defined by the ligands is constrained by symmetry at all temperatures to be 90°, although deviation of atomic positions from that mean-plane increases in the LS state as the ligand puckers. The deviation of individual atoms from the plane to be relatively small; more significant is the rotation of the whole cation, and its effect on the crystal packing, as shown in see Figure 6. This rotation may be quantified by measuring the angle between the L1-Fe mean plane and the crystallographic *ac*-plane, θ, as illustrated in Figure 6c. While θ generally increases on cooling, an abrupt increase is observed at the same temperature as the abrupt step of the spin transition. This step is concomitant with the ordering of the second perchlorate anion. The abrupt discontinuities in structural parameters (θ, unit cell volume and the *a* and *c*-parameters) indicate the presence of an isostructural crystallographic phase transition (in which an abrupt and significant structural transition is observed, but the symmetry of both phases is equivalent) accompanying the abrupt portion of the SCO.

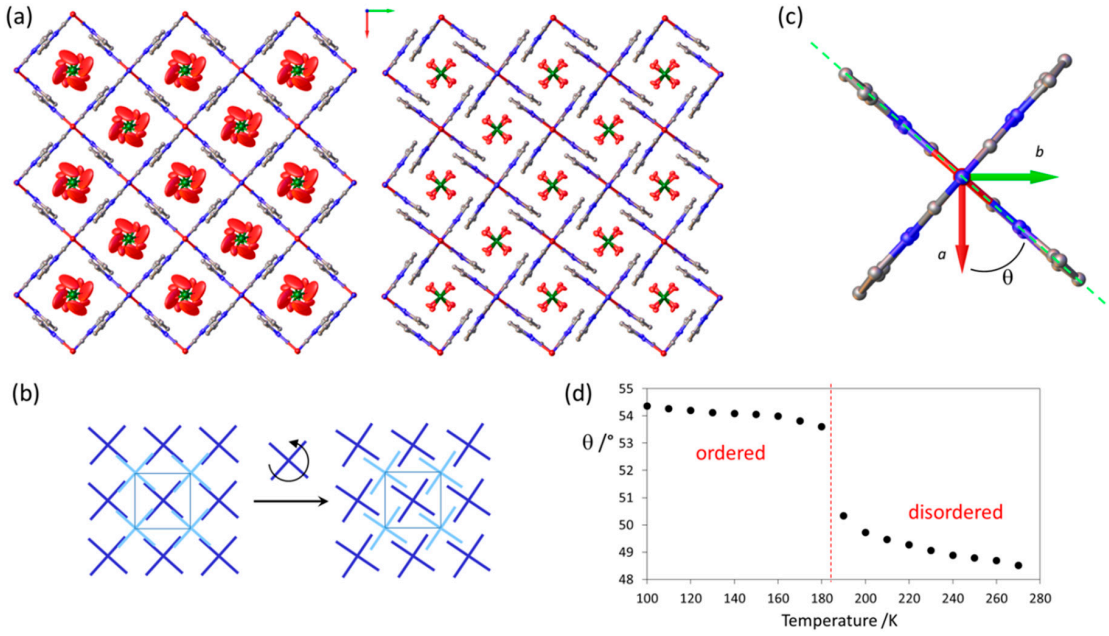

Figure 6. (**a**) Views of **1** at 270 K (left) and 100 K (right) down the *c*-axis, highlighting the rotation of the Fe complex during spin crossover (SCO), leading to a reduction in volume of the region occupied by the counterions and thus reducing dynamic disorder of the second perchlorate ion. Atomic displacement parameters are drawn at 50% for the perchlorate ions, a ball and stick model is used for all other atoms; (**b**) Illustration of the rotation mechanism for the Fe complex during the first step of the SCO. Color indicates height in the *c*-direction; (**c**) Orientation of the molecule relative to the a-axis at 270 K and definition of the θ angle between the mean-plane defined by the non-hydrogen atoms of one L1 ligand and the central iron atom (illustrated with green dashed line) and the *ac*-plane; (**d**) Evolution of the θ angle as a function of temperature, with the relative ordering of the second perchlorate ion indicated.

2.3. High Pressure X-ray Diffraction

The structure of **1** was determined at 9 pressures between ambient pressure and 20 kbar. As in the case of the variable temperature study, the symmetry remained the same at all pressures. Again, the order–disorder transition observed in the thermal study is also observed as a function of pressure, with structures at 8.32 kbar and below showing disorder of the second perchlorate ion, while those at 9.86 kbar and higher show both anions as fully ordered. Within the experimental error of the pressure determination method, this is in accordance with the variable pressure Raman spectroscopic study, where the abrupt step in the pressure-induced SCO is located around 10 kbar. The Fe-N_6 volume (Figure 7a) and the unit cell parameters as a function of pressure (Figure 7b) reveal a similar pattern to those in the thermal study, with the c-axis increasing with the abrupt step in the SCO, while the a-axis decreases.

The θ angle as a function of pressure (Figure 7c) does not show the discontinuity observed in the variable temperature study, although once the anion becomes fully ordered, the θ angle does not decrease further, despite the application of an additional 10 kbar of pressure. The maximum value of θ observed during the high pressure study is very similar to that of the thermal study (54.2° and 54.3° respectively), thus it would appear that that represents the maximum possible rotation of the cation that the lattice can accommodate. This finding may serve to explain the unusual nature of the spin transition observed in this material. A spin transition of all molecules via the isostructural phase transition associated with the abrupt part of the curve is not possible as the lattice cannot accommodate the required rotation. Thus, once the maximum possible rotation is achieved and this collective (cooperative) movement ceases, the remaining HS centers undergo gradual SCO without

cooperative motion. The fact that the disorder of the perchlorate ceases at the maximum possible rotation is perhaps not surprising. The additional space occupied by the tumbling anion is required to enable the $[FeL1_2]^{2+}$ cation to rotate, and once that tumbling has ceased there is no further space within the lattice to allow the cooperative molecular rotation.

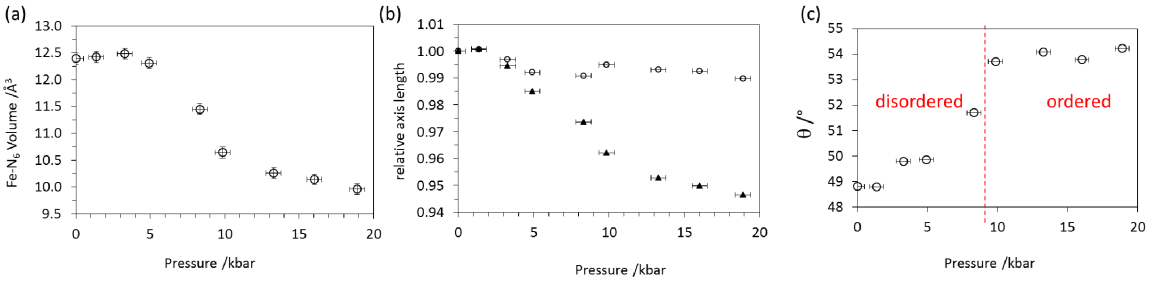

Figure 7. (**a**) Fe-N_6 volume as a function of pressure; (**b**) Evolution of the *a*- (▲) and *c*- (○) axes as a function of pressure, normalized to the ambient pressure value; (**c**) Evolution of the θ angle as a function of pressure, with the relative ordering of the second perchlorate ion indicated. Where not shown, error bars are contained within the points.

3. Experimental Section

CAUTION: while we have experienced no difficulty in handling the perchlorate salt in this study, metal-organic perchlorates are potentially explosive and should be handled with due care in small quantities, especially during high pressure work. The synthesis and analysis of the crystalline sample **1** used in this study has been reported previously [12].

Raman spectra were acquired using a 50× long working distance objective on a Jobin Yvon HR 640 micro Raman module (HORIBA Jobin Yvon IBH Ltd., Glasgow, UK), attached to an Olympus microscope (BX40) (Olympus, Southend-on-Sea, UK). The excitation source was a 632.8 nm laser. For variable temperature experiments the temperature was controlled with a Linkam THMS600 (Linkam Scientific Instruments Ltd., Tadworth, UK) thermal stage. The same crystal was used for all experiments in the variable temperature Raman spectroscopy study.

Pressure was generated using a Merrill-Basset type screw-driven diamond anvil cell (DAC) as described previously [19]. Fluoroinert FC-77 (Sigma-Aldrich, St. Louis, MO, USA) was used as the pressure transmitting medium, and the gasket was made from stainless steel. Pressure was determined using the ruby fluorescence method [20].

Variable temperature X-ray diffraction data at ambient pressure were collected on an Oxford Diffraction Gemini diffractometer (Oxford Diffraction Ltd., Abingdon, UK) using a graphite-monochromated Mo source. The temperature was controlled using an Oxford Instruments Cryojet (Oxford Instruments, Oxfordshire, UK). One single crystal was used for all XRD experiments in the variable temperature study. Data were integrated using CrysalisPro [21]. Structures were solved by direct methods using SHELXS and refined via full-matric least squares on F^2 using SHELXL [22].

High pressure X-ray diffraction experiments were carried out at beamline 11.3.1 at the Advanced Light Source, Lawrence Berkeley National Laboratory, USA using the same DAC as described above. Data were collected using a Bruker D8 with PHOTON 100 detector (Bruker AXS Inc., Madison, WI, USA, 2014) at a wavelength of 0.6702 Å (datasets between 1.37 and 13.29 kbar inclusive) or 0.6888 Å (at 16.03 and 18.90 kbar). The change in wavelength was required to provide increased flux at the highest pressures. High pressure data were integrated using the APEX2 software suite [23]. Shielding of the diffraction pattern by the DAC was dealt with by the generation of dynamic masks using a program written by Professor S. Parsons [24]. Datasets were merged using XPREP and a multiscan absorption correction was performed using SADABS [25]. Data were refined against a previously determined room temperature structure by full-matrix least squares on F^2 using SHELXL.

CCDC 1446432-1446456 contain the supplementary crystallographic data for this paper. Olex2 [26] was used as an interface to all SHELX programs. In both the variable temperature and high pressure studies, crystals were found to be merohedrally twinned about the two-fold axis of the tetragonal unit cell as described previously [13]; further details can be found in the crystallographic information files.

4. Conclusions

This study represents the first high pressure study of a SCO material with an order–disorder transition. The profile of the transition in **1** as a function of pressure was analyzed using both Raman spectroscopy and single crystal X-ray diffraction, and found to be remarkably similar to the thermal transition: and abrupt initial spin transition concomitant with an isostructural phase transition followed by a more gradual SCO of the remaining HS molecules.

A mechanism has been proposed to account for those observations involving the rotation of the $[FeL1_2]^{2+}$ cation relative to the unit cell axis (θ), which is associated with the isostructural phase transition of the initial abrupt step. As θ increases, the pocket in which the disordered perchlorate ion resides reduces in size, providing less room for the dynamic tumbling process observed at higher temperatures (and lower pressures). At a certain critical size (induced either by applying pressure or reducing temperature), the disorder ceases, and no further rotation of the cation is possible, effectively limiting the capacity of the lattice to accommodate the strain generated by the isostructural phase transition. As the transition is not complete before this cooperative rotation is obstructed, the remaining HS centers undergo gradual, non-cooperative SCO to the LS state.

Acknowledgments: This work was funded by the EPSRC (EP/K012568/1 and EP/K012576/1). The high pressure facilities at the ALS, including the laser miller and the ruby fluorescence spectrometer, are supported by COMPRES, the Consortium for Materials Properties Research in Earth Sciences under NSF Cooperative Agreement EAR 11-57758. The Advanced Light Source is supported by the Director, Office of Science, Office of Basic Energy Sciences, of the U.S. Department of Energy under Contract No. DE-AC02-05CH11231.

Author Contributions: HJS performed all Raman and variable temperature crystallographic experiments in the study, analyzed data and wrote the paper. HJS, LEH, JVK, MJB, KJG and SJT performed high pressure X-ray diffraction experiments and interpreted the data. GT analyzed and interpreted Raman data. RK synthesized the material. PRR and MAH initiated the research project.

Conflicts of Interest: The authors declare no conflict of interest.

References

1. Halcrow, M.A. Structure:function relationships in molecular spin-crossover complexes. *Chem. Soc. Rev.* **2011**, *40*, 4119–4142. [CrossRef] [PubMed]
2. Shepherd, H.J.; Palamarciuc, T.; Rosa, P.; Guionneau, P.; Molnár, G.; Letard, J.-F.; Bousseksou, A. Antagonism between Extreme Negative Linear Compression and Spin Crossover in $[Fe(dpp)_2(NCS)_2]\cdot$ py. *Angew. Chem. Int. Ed.* **2012**, *51*, 3910–3914. [CrossRef] [PubMed]
3. Nishino, M.; Boukheddaden, K.; Konishi, Y.; Miyashita, S. Simple Two-Dimensional Model for the Elastic Origin of Cooperativity among Spin States of Spin-Crossover Complexes. *Phys. Rev. Lett.* **2007**, *98*, 247203. [CrossRef] [PubMed]
4. Murray, K.S.; Kepert, C.J. Cooperativity in Spin Crossover Systems: Memory, Magnetism and Microporosity. In *Spin Crossover in Transition Metal Compounds I*; Gütlich, P., Goodwin, H.A., Eds.; Springer: Heidelberg, Germany, 2004; Volume 233, pp. 195–228.
5. Koenig, E.; Ritter, G.; Kulshreshtha, S.K.; Nelson, S.M. The high-spin ($^5T_2$) → low-spin ($^1A_1$) transition in solid tris(2,2′-bi-2-imidazoline)iron(II) diperchlorate. Hysteresis effects, simultaneous change of spin and lattice characteristics, and order-disorder phenomena of the perchlorate anion. *Inorg. Chem.* **1982**, *21*, 3022–3029. [CrossRef]
6. Matouzenko, G.S.; Bousseksou, A.; Borshch, S.A.; Perrin, M.; Zein, S.; Salmon, L.; Molnár, G.; Lecocq, S. Cooperative Spin Crossover and Order-Disorder Phenomena in a Mononuclear Compound $[Fe(DAPP)(abpt)](ClO_4)_2$ [DAPP = [Bis(3-aminopropyl)(2-pyridylmethyl)amine], abpt = 4-Amino-3,5-bis(pyridin-2-yl)-1,2,4-triazole]. *Inorg. Chem.* **2004**, *43*, 227–236. [CrossRef] [PubMed]

7. Sheu, C.F.; Pillet, S.; Lin, Y.-C.; Chen, Y.-C.; Chen, S.M.; Hsu, I.-J.; Lecomte, C.; Wang, Y. Magnetostructural Relationship in the Spin-Crossover Complex *t*-{Fe(abpt)$_2$[N(CN)$_2$]$_2$}: Polymorphism and Disorder Phenomenon. *Inorg. Chem.* **2008**, *47*, 10866–10874. [CrossRef] [PubMed]
8. Craig, G.A.; Sánchez-Costa, J.; Roubeau, O.; Teat, S.J.; Aromí, G. Coupled Crystallographic Order-Disorder and Spin State in a Bistable Molecule: Multiple Transition Dynamics. *Chem. Eur. J.* **2011**, *17*, 3120–3127. [CrossRef] [PubMed]
9. Chernyshov, D.; Klinduhov, N.; Törnroos, K.W.; Hostettler, M.; Vangdal, B.; Bürgi, H.B. Coupling between spin conversion and solvent disorder in spin crossover solids. *Phys. Rev. B* **2007**, *76*, 014406. [CrossRef]
10. Kershaw Cook, L.J.; Halcrow, M.A. Synthesis of 4-Hydroxy-2,6-di(pyrazol-1-yl)pyridine, and the Spin State Behaviour of Its Iron(II) Complex Salts. *Magnetochemistry* **2015**, *1*, 3–16. [CrossRef]
11. Murray, K.S. *Spin-Crossover Materials: Properties and Applications*; Wiley: Chichester, UK, 2013; pp. 1–54.
12. Elhaïk, J.; Money, V.A.; Barrett, S.A.; Kilner, C.A.; Radosavljevic Evans, I.; Halcrow, M.A. The spin-states and spin-crossover behaviour of iron(II) complexes of 2,6-dipyrazol-1-ylpyrazine derivatives. *Dalton Trans.* **2003**. [CrossRef]
13. Money, V.A.; Elhaïk, J.E.; Radosavljevic Evans, I.; Halcrow, M.A.; Howard, J.A.K. A study of the thermal and light induced spin transition in [FeL$_2$](BF$_4$)$_2$ and [FeL$_2$](ClO$_4$)$_2$ L = 2,6-di(3-methylpyrazol-1-yl)pyrazine. *Dalton Trans.* **2004**. [CrossRef] [PubMed]
14. Ksenofontov, V.; Gaspar, A.B.; Gutlich, P. *Spin Crossover in Transition Metal Compounds III*; Gütlich, P., Goodwin, H.A., Eds.; Springer: Heidelberg, Germany, 2004; Volume 235, pp. 23–64.
15. Tao, J.; Wei, R.-J.; Huang, R.-B.; Zheng, L.-S. Polymorphism in spin-crossover systems. *Chem. Soc. Rev.* **2012**, *41*, 703–737. [PubMed]
16. Guionneau, P.; Collet, E. *Spin-Crossover Materials: Properties and Applications*; Wiley: Chichester, UK, 2013; pp. 507–526.
17. Tuchagues, J.-P.; Bousseksou, A.; Molnár, G.; McGarvey, J.J.; Varret, F. *Spin Crossover in Transition Metal Compounds III*; Gütlich, P., Goodwin, H.A., Eds.; Springer: Heidelberg, Germany, 2004; Volume 235, pp. 85–103.
18. Halcrow, M.A. *Spin-Crossover Materials: Properties and Applications*; Wiley: Chichester, UK, 2013; pp. 147–169.
19. Woodall, C.H.; Fuertes, S.; Beavers, C.M.; Hatcher, L.E.; Parlett, A.; Shepherd, H.J.; Christensen, J.; Teat, S.J.; Intissar, M.; Rodrigue-Witchel, A.; *et al*. Tunable Trimers: Using Temperature and Pressure to Control Luminescent Emission in Gold(I) Pyrazolate-Based Trimers. *Chem. Eur. J.* **2014**, *20*, 16933–16942. [CrossRef] [PubMed]
20. Piermarini, G.J.; Block, S.; Barnett, J.D.; Forman, R.A. Calibration of the pressure dependence of the R_1 ruby fluorescence line to 195 kbar. *J. Appl. Phys.* **1975**, *46*, 2774–2780. [CrossRef]
21. *CrysAlisPro*, version 171.37.33; Oxford Diffraction Ltd.: Abingdon, UK, 2015.
22. Sheldrick, G.M. A Short History of SHELX. *Acta Crystallogr. Sect. A* **2008**, *64*, 112–122. [CrossRef] [PubMed]
23. *APEX2*, v2014.9-0; Bruker AXS Inc.: Madison, WI, USA, 2014.
24. Dawson, A.; Allan, D.R.; Parsons, S.; Ruf, M. Use of a CCD diffractometer in crystal structure determinations at high pressure. *J. Appl. Crystallogr.* **2004**, *37*, 410–416. [CrossRef]
25. *SADABS Program for Empirical Absorption Correction and Scaling of X-ray Data*; Bruker AXS Inc.: Madison, WI, USA, 2005.
26. Dolomanov, O.V.; Bourhis, L.J.; Gildea, R.J.; Howard, J.A.K.; Puschmann, H. OLEX2: A complete structure solution, refinement and analysis program. *J. Appl. Crystallogr.* **2009**, *42*, 339–341. [CrossRef]